Simulation of the hydrogen ground state in stochastic electrodynamics

Nieuwenhuizen, T.M.; Liska, M.T.P.

DOI
10.1088/0031-8949/2015/T165/014006
Publication date
2015
Document Version
Author accepted manuscript
Published in
Physica Scripta

Simulation of the hydrogen ground state in Stochastic Electrodynamics

Theo M. Nieuwenhuizen[1,2] **and Matthew T. P. Liska**[1]

[1] Institute for Theoretical Physics, University of Amsterdam, P.O. Box 94485, 1098 XH Amsterdam, the Netherlands

[2] International Institute of Physics, UFRG, Av. O. Gomes de Lima, 1722, 59078-400 Natal-RN, Brazil

E-mail: t.m.nieuwenhuizen@uva.nl

Abstract. Stochastic electrodynamics is a classical theory which assumes that the physical vacuum consists of classical stochastic fields with average energy $\frac{1}{2}\hbar\omega$ in each mode, i.e., the zero-point Planck spectrum. While this classical theory explains many quantum phenomena related to harmonic oscillator problems, hard results on nonlinear systems are still lacking. In this work the hydrogen ground state is studied by numerically solving the Abraham – Lorentz equation in the dipole approximation. First the stochastic Gaussian field is represented by a sum over Gaussian frequency components, next the dynamics is solved numerically using OpenCL. The approach improves on work by Cole and Zou 2003 by treating the full $3d$ problem and reaching longer simulation times. The results are compared with a conjecture for the ground state phase space density. Though short time results suggest a trend towards confirmation, in all attempted modelings the atom ionises at longer times.

PACS numbers: 11.10, 05.20, 05.30, 03.65

Keywords: Stochastic electrodynamics, hydrogen ground state, numerical simulation

arXiv:1407.7030

1. Introduction

The theory called Stochastic Electrodynamics (SED) starts with a classical picture of what is normally called the quantum vacuum: the vacuum is assumed to consist of fluctuating classical electrodynamic fields with energy per eigenmode equal to $\frac{1}{2}\hbar\omega$, which adds up to the zero-point Planck spectrum $\rho(\omega) = \hbar\omega^3/2\pi^2c^3$. Particles are considered as classical too, hence in the hydrogen problem the electron is a point particle that essentially goes around the nucleus in Kepler orbits. Like any accelerated classical charge it radiates, hence the energy loss causes it to fall onto the nucleus, the old problem of the classical atomic model. The assertion of SED is that this energy loss is statistically compensated by energy gained from the fluctuating vacuum fields, so that the stability of the hydrogen atom, and more generally of matter, is achieved.

SED has enjoyed popularity in the seventies and eighties of last century, when many linear problems (harmonic oscillator problems) could be reproduced from this classical approach [1, 2]. The field lost attention when it became clear that nonlinear problems, such as the hydrogen stability, could not be explained. For instance, from a Fokker-Planck analysis it was concluded that the electron would evaporate, thus self-ionising the H atom [1]. Outside the field, the theory is considered as suspicious due to the supposed road block for hidden variables theories by Bell inequalities. The latter will not be our concern, since one of us has joined a growing group of researchers who are convinced that Bell had to make a hidden, unnatural assumption to derive his inequalities, a problem related to the context (setup of detectors).‡ So the issue of Bell inequality violations should not be held against SED.

Not withstanding the above and other apparent setbacks, several people have continued to develop SED. de la Peña and Cetto wrote a book [1] on it in 1996 and a second one [4], with Valdes-Hernandes, was recently published. They have formulated both a Heisenberg and a Schrödinger approach arriving at the familiar equations of QM. They also consider the problem of entanglement, it being carried by the stochastic field [5, 6]; this seems akin to the creation of two polarons where lattice distortions (phonons) move with the two electrons. França et al. also derive the Schrödinger equation and stress the role of the ZPF in the uncertainly relations and the photo-electric effect [7]. One of us considers in SED and SED-like theories a "pull back" mechanism to turn classical scattering into quantum scattering [8]; the phase space densities of various states of the relativistic hydrogen atom [9]; and an arrow of time: The involved energy current (fluctuation energy in, radiation energy out) would define the *subquantum arrow of time*, intimately connected to the stability of matter. It is more fundamental than

‡ Although Bell assumed that different contexts can be combined, this is not true in general, hence it leads to the *contextuality loophole*, which cannot be closed for it being a theoretical problem [3]. Violation of the Bell inequality demonstrates that the combination of contexts is not allowed, without any further implication on presence or absence of local realism.

the entropic and cosmological arrows of time [10].

In view of these aspects, we see it as crucial to test SED on a nonlinear problem. The most obvious case is the hydrogen ground state. While unstable in the Fokker-Planck approximation [11, 1], the treatment of de la Peña and Cetto points to resonances. In the diagrammatic approach of the Liouville equation by [12], one of us noticed that higher order corrections in the fine structure constant achieve power laws in time, so that in the long time limit neither stability nor instability is obvious [13].

Lacking analytical derivations it would be desirable to find results from numerical analysis, the first target being the hydrogen ground state. This challenge is taken up in 2003 by Cole and Zou [14]. They discretize the stochastic field and follow the perturbed Kepler orbits up to 7.252 ps, that is, up to 300,000 Bohr periods. Taking the average over 11 simulated trajectories, they establish an encouraging fit of the radial ground state density.

With computing power having strongly increased during last decade, it seems appropriate to redo the simulations. We take up this challenge and compare the results with the conjecture for the phase space density of the ground state [9]. This theory will be recalled in section 2. In section 3 we recall the conjecture for the phase space density and express this as a conjecture for the distribution of conserved quantities energy and angular momentum. The simulation results will be reported in section 4. We close with a discussion. The appendix gives some details about our code in OpenCL.

2. The hydrogen problem in stochastic electrodynamics

The Newton equation for the electron with damping and noise, also called the Abraham-Lorentz equation or Brafford-Marshall equation, reads

$$m\ddot{\mathbf{r}} = -\frac{Ze^2\mathbf{r}}{4\pi\epsilon_0 r^3} + \frac{e^2}{6\pi\epsilon_0 c^3}\,\dddot{\mathbf{r}} - e[\mathbf{E}(\mathbf{r},t) + \dot{\mathbf{r}}\times\mathbf{B}(\mathbf{r},t)] \tag{1}$$

where $\mathbf{r} = \mathbf{r}(t)$ is the orbit and we stress the explicit time-dependence of $\mathbf{E}$ and $\mathbf{B}$. The first term on the right hand side is the Coulomb force on a charge $-e$ by a central charge Ze, the second the damping term, which arises together with a renormalisation of the mass, so that m is the physical mass of the electron.

The conserved quantities of the unperturbed problem are the energy, angular momentum and the Lagrange-Runge-Lenz eccentricity vector,

$$\mathcal{E} = \frac{\mathbf{p}^2}{2m} - \frac{Ze^2}{4\pi\epsilon_0 r}, \qquad \mathbf{L} = \mathbf{r}\times\mathbf{p}, \quad \boldsymbol{\varepsilon} = \frac{1}{m}\mathbf{p}\times\mathbf{L} - \frac{Ze^2}{4\pi\epsilon_0}\hat{\mathbf{r}}. \tag{2}$$

The vector potential and the electric and magnetic fields are sums of plane waves with random coefficients

$$\mathbf{A} = \sum_{\mathbf{k},\lambda} \sqrt{\frac{\mathcal{E}_\mathbf{n}}{\epsilon_0 L_x L_y L_z}}\, \frac{\hat{\varepsilon}_{\mathbf{n}\lambda}}{\omega_\mathbf{n}} [A_{\mathbf{n}\lambda} \sin(\mathbf{k}\cdot\mathbf{r} - \omega_\mathbf{n} t) + B_{\mathbf{n}\lambda} \cos(\mathbf{k}\cdot\mathbf{r} - \omega_\mathbf{n} t)]$$

$$\mathbf{E} = \sum_{\mathbf{k},\lambda} \sqrt{\frac{\mathcal{E}_\mathbf{n}}{\epsilon_0 L_x L_y L_z}}\, \hat{\varepsilon}_{\mathbf{n}\lambda} [A_{\mathbf{n}\lambda} \cos(\mathbf{k}\cdot\mathbf{r} - \omega_\mathbf{n} t) - B_{\mathbf{n}\lambda} \sin(\mathbf{k}\cdot\mathbf{r} - \omega_\mathbf{n} t)] \quad (3)$$

$$\mathbf{B} = \sum_{\mathbf{k},\lambda} \sqrt{\frac{\mu_0 \mathcal{E}_\mathbf{n}}{L_x L_y L_z}}\, \hat{\mathbf{k}} \times \hat{\varepsilon}_{\mathbf{n}\lambda} [A_{\mathbf{n}\lambda} \cos(\mathbf{k}\cdot\mathbf{r} - \omega_\mathbf{n} t) - B_{\mathbf{n}\lambda} \sin(\mathbf{k}\cdot\mathbf{r} - \omega_\mathbf{n} t)]$$

Since we adopt periodic boundary conditions, the wave vector components $k_a = 2\pi n_a / L_a$ involve integer $n_a = -\infty, \cdots, -1, 0, 1, \cdots, \infty$, $(a = x, y, z)$. The $\hat{\varepsilon}_{\mathbf{n}\lambda}$ with $(\lambda = 1, 2)$ are polarisation vectors. The $A_{\mathbf{n}\lambda}$ and $B_{\mathbf{n}\lambda}$ are independent random Gaussian variables with average zero and unit variance. For each term the energy $\int_V \mathrm{d}^3 r (\frac{\epsilon_0}{2}\mathbf{E}^2 + \frac{1}{2\mu_0}\mathbf{B}^2)$ is in integral equal to $\mathcal{E}_\mathbf{n}$, for which we choose the zero point energy combined with an exponential cutoff at the electron zero point energy, $\mathcal{E}_\mathbf{n} = \frac{1}{2}\hbar\omega_\mathbf{n} \exp(-\hbar\omega_\mathbf{n}/mc^2)$. The correlation function of the stochastic electric field is translation invariant in space and time. We shall need

$$C_{ij}^{EE}(\mathbf{0}, t) = \langle E_i(\mathbf{r}, t) E_j(\mathbf{r}, 0)\rangle = \delta_{ij} \frac{\hbar}{\pi^2 \epsilon_0 c^3}\, \Re \frac{1}{(t + i\hbar/mc^2)^4} \quad (4)$$

For our application to the H atom, we go to Bohr units,

$$a_0 = \frac{\hbar}{Z\alpha mc}, \qquad \tau_0 = \frac{1}{\omega_0} = \frac{\hbar}{Z^2\alpha^2 mc^2} \quad (5)$$

τ_0 is the characteristic Bohr time and the Bohr period is $P_0 = 2\pi\tau_0$. In these units the equation of motion becomes

$$\ddot{\mathbf{r}} = -\frac{\mathbf{r}}{r^3} + \beta^2 \dddot{\mathbf{r}} - \beta[\mathbf{E}(Z\alpha\mathbf{r}, t) + Z\alpha\dot{\mathbf{r}} \times \mathbf{B}(Z\alpha\mathbf{r}, t)], \quad (6)$$

Both the fluctuations and the damping involve the small parameter §

$$\beta = \sqrt{\frac{2}{3}} Z\alpha^{3/2} = \frac{Z}{1964.71}, \qquad \alpha = \frac{e^2}{4\pi\epsilon_0\hbar c} \approx \frac{1}{137} \quad (7)$$

It is seen that the effect of $Z > 1$ is to make the fluctuations and damping stronger, suggesting a speed up in the simulations.

The phase $\mathbf{k}\cdot\mathbf{r} - \omega t$ of the plane waves of the EM fields reads in Bohr units $Z\alpha\mathbf{k}\cdot\mathbf{r} - kt$, so to leading order we may neglect the spatial dependence of the electric field (dipole approximation), while we can also omit the magnetic field. Now $\mathbf{E}(t) \equiv \mathbf{E}(\mathbf{0}, t)$ is given as in (3) at $\mathbf{r} = \mathbf{0}$, with the argument of the square root replaced by the dimensionless expression $3\pi\,\omega\tau_0\,(c\tau_0/L_a)^3$. The autocorrelation function thus reads

§ In order to have β also as prefactor of $\mathbf{E}$, we absorb a factor $\sqrt{3/2}$ in $\mathbf{A}$, $\mathbf{B}$ and $\mathbf{E}$.

$$C_{ab}^{EE}(t) = \langle E_a(t) E_b(0) \rangle = \delta_{ab} \frac{6}{\pi} \Re \frac{1}{(t - iZ^2\alpha^2)^4}, \tag{8}$$

with t expressed in Bohr times.

After iterating the damping term in Eq. (6), we arrive at

$$\ddot{\mathbf{r}} = -\frac{\mathbf{r}}{r^3} - \beta^2 \frac{\dot{\mathbf{r}} - 3(\dot{\mathbf{r}} \cdot \hat{\mathbf{r}})\hat{\mathbf{r}}}{r^3} - \beta \mathbf{E}(t), \tag{9}$$

which we may write as

$$\dot{\mathbf{p}} = \mathbf{f}(\mathbf{r}) - \beta^2 \dot{\mathbf{f}} - \beta \mathbf{E}(t), \qquad \dot{\mathbf{r}} = \mathbf{p}, \qquad \mathbf{f}(\mathbf{r}) = -\frac{\mathbf{r}}{r^3} \tag{10}$$

where $\dot{\mathbf{f}} \equiv \nabla \mathbf{f}(\mathbf{r}) \cdot \dot{\mathbf{r}}$. The conserved quantities at $\beta \to 0$ now read

$$\mathcal{E} = \frac{1}{2}\mathbf{p}^2 - \frac{1}{r}, \qquad \mathbf{L} = \mathbf{r} \times \mathbf{p}, \qquad \boldsymbol{\varepsilon} = p^2 \mathbf{r} - (\mathbf{p} \cdot \mathbf{r})\mathbf{p} - \hat{\mathbf{r}} \tag{11}$$

It follows that

$$\varepsilon^2 = 1 + 2\mathcal{E}L^2. \tag{12}$$

The relation $\boldsymbol{\varepsilon} \cdot \mathbf{r} = L^2 - r$ can be expressed as

$$r = \frac{L^2}{1 + \varepsilon \cos\phi} = \frac{(1 - \varepsilon^2)R}{2(1 + \varepsilon \cos\phi)}, \qquad R \equiv -\frac{1}{\mathcal{E}} > 0, \tag{13}$$

where ϕ is the angle between $\boldsymbol{\varepsilon}$ and $\mathbf{r}$. Thus ε expresses the eccentricity of the orbit.

2.1. Simplified representation of the stochastic field

The stochastic electric field involves the numerically demanding $3d$ sum over $\mathbf{k}$ values. To facilitate the simulations, we replace it by a simpler Gaussian field. We adopt a uniform grid in ω-space with $\Delta\omega_n = 1/N$ with $N \gg 1$, so that

$$\omega_n = \frac{n}{N}, \qquad (n = 1, 2, \cdots), \tag{14}$$

which corresponds to $(n/N)\,\omega_0$ in physical units. Next we assume for each n and for each direction $a = x, y, z$, two independent Gaussian random variables A_n^a and B_n^a, with average 0 and variance 1, and consider the $1d$ sum

$$\mathbf{E}(t) = \sum_{n=0}^{\infty} \sqrt{\frac{\Delta\omega_n\ \omega_n^3}{\pi}} e^{-\frac{1}{2}Z^2\alpha^2\omega_n} (-\mathbf{A}_n \cos\omega_n t + \mathbf{B}_n \sin\omega_n t). \tag{15}$$

Its two-point correlation function reads

$$C^{EE}_{ab}(t-s) = \delta_{ab} C_{EE}(t-s), \quad C_{EE}(t) = \frac{1}{8\pi N^4}\,\Re\,\frac{3+\sinh^2[(Z^2\alpha^2+it)/2N]}{\sinh^4[(Z^2\alpha^2+it)/2N]}. \tag{16}$$

At fixed t it reproduces in the limit $N\to\infty$ the autocorrelation function (8). For finite N, the discretization will be reliable for times up to $t\simeq N$.

The related $\mathbf{A}$ field reads

$$\mathbf{A}(t) = \sum_{n=1}^{\infty} \sqrt{\frac{\Delta\omega_n\ \omega_n}{\pi}} e^{-\frac{1}{2}Z^2\alpha^2\omega_n} (\mathbf{A}_n \sin\omega_n t - \mathbf{B}_n \cos\omega_n t), \tag{17}$$

and has two-point correlation function

$$C^{AA}_{ab}(t-s) = \delta_{ab} C_{AA}(t-s), \quad C_{AA}(t) = \frac{1}{4\pi N^2}\,\Re\,\frac{1}{\sinh^2[(Z^2\alpha^2+it)/2N]}. \tag{18}$$

2.2. Canonical momentum

For large ω_n, the coefficients of the $\mathbf{E}$ field grow as $\omega_n^{3/2}$, which may cause numerical errors. To check whether this leads to numerical inconsistencies, we formulate several presentations of the dynamics where some of the integrations are performed analytically.

Firstly, the "*canonical*" dynamics reads

$$\begin{aligned} \dot{\mathbf{r}} &= \mathbf{p} + \beta\mathbf{A} + \beta^2\mathbf{f}(\mathbf{r}), \quad \dot{\mathbf{p}} = \mathbf{f}(\mathbf{r})\,, \\ \dot{\mathbf{q}} &= \mathbf{p} + \beta\mathbf{A} + \beta^2\mathbf{f}(\mathbf{r})\,, \quad \mathbf{r} = \mathbf{q} \end{aligned} \tag{19}$$

When combined they reproduce (10); notice that one does not need $\dot{\mathbf{f}}$. The benefit is that at large n (i.e. for high harmonics), $\mathbf{A}$ has smaller coefficients than $\mathbf{E}$, inducing a better numerical stability.

The energy should not include the $\mathbf{A}^2$ term, since it is already included in the renormalised mass. With $V(r) = -\frac{1}{r}$ one has

$$\begin{aligned} \mathcal{E} &= \frac{1}{2}\mathbf{p}^2 + \beta\mathbf{p}\cdot\mathbf{A} + V(r) \\ &= \frac{1}{2}\dot{\mathbf{r}}^2 + V(r) - \frac{1}{2}\beta^2\mathbf{A}^2, \end{aligned} \tag{20}$$

For the free particle one would have $\mathbf{p} = \mathbf{p}_0 =$ constant, and $\langle\mathcal{E}\rangle = \frac{1}{2}\mathbf{p}_0^2$.

2.3. Grand canonical momentum

We may proceed on this track. Define $\mathbf{C} = \int^t \mathrm{d}t\mathbf{A}$, which amounts to

$$\mathbf{C}(t) = \sum_{n=1}^{\infty} \sqrt{\frac{\Delta\omega_n}{\pi\omega_n}}\,(-\mathbf{A}_n \cos\omega_n t + \mathbf{B}_n \sin\omega_n t)\,, \tag{21}$$

and the canonical momentum $\mathbf{p} \equiv \int^t \mathrm{d}t\, \mathbf{f}$ and the canonical position $\mathbf{q} = \int^t \mathrm{d}t\, (\mathbf{p} + \beta^2 \mathbf{f})$. Then, consider the dynamics for $\mathbf{p}$, $\mathbf{q}$, using the physical position $\mathbf{r}$,

$$\begin{aligned} \dot{\mathbf{p}} &= \mathbf{f}(\mathbf{r}), \qquad \dot{\mathbf{q}} = \mathbf{p} + \beta^2 \mathbf{f}(\mathbf{r}), \\ \mathbf{r} &= \mathbf{q} + \beta \mathbf{C}, \qquad \dot{\mathbf{r}} = \dot{\mathbf{q}} + \beta \mathbf{A}. \end{aligned} \tag{22}$$

This is a "*pure grand canonical*" system of 6 first order equations, equivalent to the Newton problem (10). The initial conditions can be taken by neglecting β, so that $\mathbf{q}(0) = \mathbf{r}(0)$; $\mathbf{p}(0) = \dot{\mathbf{r}}(0)$. The physical speed entering $\mathcal{E}$ and L is $\dot{\mathbf{r}} = \dot{\mathbf{q}} + \beta \dot{\mathbf{C}} = \mathbf{p} + \beta \mathbf{A} + \beta^2 \mathbf{f}$; this extra evaluation of $\mathbf{A}$ is needed at most once per orbit.

2.3.1. Grand canonical momentum: second order differential equation In the above approach let us express $\ddot{\mathbf{r}} = \mathbf{f} - \beta \mathbf{E} + \beta^2 \dot{\mathbf{f}}$ by a variable $\mathbf{s}$ through the definition $\mathbf{q} = \mathbf{s} + \beta^2 \mathbf{p}$,

$$\dot{\mathbf{p}} = \mathbf{f}(\mathbf{r})\,, \qquad \dot{\mathbf{s}} = \mathbf{p}\,, \qquad \mathbf{r} = \mathbf{s} + \beta^2 \mathbf{p} + \beta \mathbf{C}, \tag{23}$$

They combine into a second order differential equation for $\mathbf{s}$,

$$\ddot{\mathbf{s}} = \mathbf{f}(\mathbf{r}), \quad \mathbf{r} = \mathbf{s} + \beta \mathbf{C} + \beta^2 \dot{\mathbf{s}}. \tag{24}$$

2.3.2. Mixed grand canonical ensemble: Splitting up in low and high frequency components. If one splits into low frequencies $\omega_n \leq \omega_*$ and high frequencies $\omega_n > \omega_*$

$$\mathbf{C} = \mathbf{C}_l + \mathbf{C}_h \tag{25}$$

one may define $\mathbf{u}$ by

$$\mathbf{s} = \mathbf{u} - \beta \mathbf{C}_l \tag{26}$$

and get the dynamics

$$\begin{aligned} \ddot{\mathbf{u}} &= \mathbf{f}(\mathbf{r}) - \beta \mathbf{E}_l, \\ \mathbf{r} &= \mathbf{u} + \beta^2 \dot{\mathbf{u}} + \beta \mathbf{C}_h - \beta^3 \mathbf{A}_l \approx \mathbf{u} + \beta^2 \dot{\mathbf{u}} + \beta \mathbf{C}_h \end{aligned} \tag{27}$$

The frequency components of $\mathbf{E}_l$ for $\omega_n \to 0$ and $\mathbf{C}_h$ for $\omega_n \to \infty$ have small amplitudes.

2.3.3. Fixed number of harmonics, moving number of frequency components When working with a fixed number of harmonics, say $n_h = 2.5$, and floating $\omega_m = n_h k^3$, a change is needed in the equation of motion (24) when the cutoff frequency ω_m is updated because k has changed noticibly. Indeed, both the electron position $\mathbf{r}$ and its speed $\dot{\mathbf{r}}$ should not alter by the update. Because of the form (23), it is natural to assume that $\mathbf{s}$, $\dot{\mathbf{s}}$ and $\ddot{\mathbf{s}}$ are continuous.

Let us start at time $t_0 = 0$ with N_0 terms in the sum. At a time t_1 this is changed to N_1, and successively to N_{k+1} at times t_{k+1} for $k = 1, 2 \cdots$. Let us write in the time interval $t_k < t < t_{k+1}$

$$\begin{aligned} \mathbf{r} &= \mathbf{s} + \beta^2 \dot{\mathbf{s}} + \beta \mathbf{C}(t, N_k) - \beta(\mathbf{u}_k + \mathbf{v}_k t), \\ \dot{\mathbf{r}} &= \dot{\mathbf{s}} + \beta^2 \ddot{\mathbf{s}} + \beta \mathbf{A}(t, N_k) - \beta \mathbf{v}_k, \quad (t_k < t < t_{k+1}) \end{aligned} \tag{28}$$

At t_k the fields $\mathbf{C}$ and $\mathbf{A} = \dot{\mathbf{C}}$ make a step due to taking N_k terms instead of N_{k-1}, viz.

$$\begin{aligned} \Delta \mathbf{C}_k &= \mathbf{C}(t_k, N_k) - \mathbf{C}(t_k, N_{k-1}), \\ \Delta \mathbf{A}_k &= \mathbf{A}(t_k, N_k) - \mathbf{A}(t_k, N_{k-1}), \end{aligned} \tag{29}$$

Continuity of $\mathbf{r}$ and $\dot{\mathbf{r}}$ at time t_k then requires

$$\begin{aligned} \mathbf{u}_k &= \mathbf{u}_{k-1} + \Delta \mathbf{C}_k - \Delta \mathbf{A}_k t_k, \\ \mathbf{v}_k &= \mathbf{v}_{k-1} + \Delta \mathbf{A}_k \end{aligned} \tag{30}$$

One starts with $\mathbf{u}_0 = \mathbf{v}_0 = 0$, so that

$$\mathbf{u}_k + \mathbf{v}_k t = \sum_{l=1}^{k} \Delta \mathbf{C}_l + \sum_{l=1}^{k} \Delta \mathbf{A}_l (t - t_l), \qquad (t_k < t < t_{k+1}), \tag{31}$$

$$\mathbf{u}(t) + \mathbf{v}(t) t = \sum_{l=1}^{\infty} \theta(t - t_l) [\, \Delta \mathbf{C}_l + \Delta \mathbf{A}_l (t - t_l) \,] \tag{32}$$

Since $\mathbf{r}$ is continuous, so is $\ddot{\mathbf{s}} = \mathbf{f}(\mathbf{r})$, as assumed. Also $\dddot{\mathbf{s}} = \nabla \mathbf{f} \cdot \dot{\mathbf{r}}$ will be continuous. From $\ddot{\mathbf{r}} = \ddot{\mathbf{s}} + \beta^2 \dddot{\mathbf{s}} - \beta \mathbf{E}(t, N_k)$ it is seen that $\ddot{\mathbf{r}}$ discontinuous, as it is in the standard form of the Newton equation $\ddot{\mathbf{r}} = \mathbf{f}(\mathbf{r}) - \beta \mathbf{E} + \beta^2 \nabla \mathbf{f} \cdot \dot{\mathbf{r}}$.

The $\mathbf{v}_k t$ shift in $\mathbf{r}$ is possibly dangerous, since at large t it may lead to large $|\mathbf{r}|$.

2.4. Mixed grand canonical ensemble

In this scheme the high frequency components of the noise $\mathbf{C}$ have decaying amplitude, but the small frequency part is strong, which does not do justice to the physics either. To avoid this aspect, one may consider a combination of the two themes. First, split up $\mathbf{A}$ in "smaller" and "greater" frequency components,

$$\mathbf{A} = \mathbf{A}_s + \dot{\mathbf{C}}_g,$$

$$\mathbf{A}_s = \sum_{n=1}^{N_1} \sqrt{\frac{n}{\pi N^2}} (\mathbf{A}_n \sin \frac{nt}{N} + \mathbf{B}_n \cos \frac{nt}{N}), \tag{33}$$

$$\dot{\mathbf{C}}_g = \sum_{n=N_1+1}^{\infty} \sqrt{\frac{n}{\pi N^2}} (\mathbf{A}_n \sin \frac{nt}{N} + \mathbf{B}_n \cos \frac{nt}{N}), \tag{34}$$

(35)

Consider the "*mixed grand canonical*" dynamics for the canonical momentum $\mathbf{p}$, a modified canonical position $\mathbf{q}$ and the physical position $\mathbf{r}$,

$$\dot{\mathbf{p}} = \mathbf{f}(\mathbf{r}), \qquad \dot{\mathbf{q}} = \mathbf{p} + \beta\mathbf{A}_s + \beta^2\mathbf{f}(\mathbf{r}), \qquad \mathbf{r} = \mathbf{q} + \beta\mathbf{C}_g \tag{36}$$

This implies the physical momentum $\dot{\mathbf{r}} = \mathbf{p} + \beta(\mathbf{A}_s + \dot{\mathbf{C}}_g) + \beta^2\mathbf{f}$.
These also combine to Eq. (10). The benefit is that both $\mathbf{A}_s$ and $\mathbf{C}_g$ are well-behaved sums with maximal coefficients at $n = N_1$ for $\mathbf{A}_s$ and at $n = N_1 + 1$ for $\mathbf{C}_g$. The most logical choice is the fixed case N_1. One may choose $N_1 = N$; even better is $N_1 = (2/3)^{3/2}N = 0.5443N$, which puts $\omega_{N_1} = k_m^3$ at $\mathcal{E}_m = -\frac{1}{2}k_m^2 = -\frac{1}{3}$ where $P(\mathcal{E})$ is maximal. It would not change much to take just $N_1 = \frac{1}{2}N$.

2.4.1. Final dynamics: changing N_1 and N_2 The present argument remains valid for numerical approaches, where we have to approximate $\mathbf{C} \equiv \mathbf{C}_g$ as a finite sum, $\mathbf{C}_g = \sum_{N_1+1}^{N_2} \mathbf{C}_n$, and N_1 and N_2 are updated simultaneously. Let us assume that this covers $n_h + \frac{1}{2}$ harmonics of the orbit, with $n_h = 2$ or 4, or $\cdots$. At the initial time we set $N_2 = (n_h + \frac{1}{2})k^3N$, next to $N_1 = k^3N$.

At some later time t' where k has evolved to some k' we may wish to update not only N_1 but also N_2, to become $N_1' = k'^3N$ and $N_2' = (n_h + \frac{1}{2})k'^3N$. This change is also covered in the above formulae, where now $\mathbf{C}$ involves limits $N_1 + 1$ and N_2 before t' while the update $\mathbf{C}'$ involves limits $N_1' + 1$ and N_2' after t'. Likewise, $\mathbf{A}$ involves limits 1 and N_1, and $\mathbf{A}'$ involves limits 1 and N_1'.

All by all, the dynamics can general be described by

$$\begin{aligned} \dot{\mathbf{p}} \quad &= \mathbf{f}(\mathbf{r})\,,\ \dot{\mathbf{q}}(t) = \mathbf{p} + \beta^2\mathbf{f} + \beta[\mathbf{A}'(t) + \delta\mathbf{A}]\,, \\ \mathbf{r}(t) &= \mathbf{q}(t) + \beta[\mathbf{C}'(t) + \delta\mathbf{C}] \end{aligned} \tag{37}$$

In the initial period, one just has $\delta\mathbf{A} = \delta\mathbf{C} = 0$ while $\mathbf{A}' = \mathbf{A}$, $\mathbf{C}' = \mathbf{C}$ are given by

$$\begin{aligned} \mathbf{A} &= \sum_{n=1}^{N_1} \sqrt{\frac{n}{\pi N^2}}(\mathbf{A}_n \sin\frac{nt}{N} + \mathbf{B}_n \cos\frac{nt}{N}), \\ \mathbf{C} &= \sum_{n=N_1+1}^{N_2} \sqrt{\frac{1}{\pi n}}(-\mathbf{A}_n \cos\frac{nt}{N} + \mathbf{B}_n \sin\frac{nt}{N}) \end{aligned} \tag{38}$$

After the first change of N_1 and N_2 one works with the updates $\mathbf{A}'$ and $\mathbf{C}'$, which involve N_1' and N_2', rather than N_1 and N_2, respectively. Matching at t' yields

$$\begin{aligned} \delta\mathbf{A} &= \mathbf{A}(t') - \mathbf{A}'(t') + \dot{\mathbf{C}}(t') - \dot{\mathbf{C}}'(t'), \\ \delta\mathbf{C} &= \mathbf{C}(t') - \mathbf{C}'(t') \end{aligned} \tag{39}$$

For subsequent changes of N_1, N_2 one repeats this schedule. One must add the new shifts to the previous ones,

$$\begin{aligned}\delta\mathbf{A}_{new} &= \delta\mathbf{A}_{old} + \mathbf{A}(t') - \mathbf{A}'(t') + \dot{\mathbf{C}}(t') - \dot{\mathbf{C}}'(t')\,,\\ \delta\mathbf{C}_{new} &= \delta\mathbf{C}_{old} + \mathbf{C}(t') - \mathbf{C}'(t')\end{aligned} \tag{40}$$

which amounts in total to

$$\begin{aligned}\delta\mathbf{A} &= \sum_{t'<t}[\mathbf{A}(t') - \mathbf{A}'(t') + \dot{\mathbf{C}}(t') - \dot{\mathbf{C}}'(t')]\\ \delta\mathbf{C} &= \sum_{t'<t}[\mathbf{C}(t') - \mathbf{C}'(t')].\end{aligned} \tag{41}$$

These forms have been applied to test the results of our simulations.

3. Conjecture for the ground state phase space density

For a dynamics with weak noise the stationary distribution in phase space must be a function of the conserved quantities, here the seven parameters $\mathcal{E}$, $\mathbf{L}$ and ε. They contain the scalars $\mathcal{E}$, L and ε, while the coordinate-invariant inner product $\mathbf{L}\cdot\boldsymbol{\varepsilon}$ vanishes. Because of the relation (12), two of the scalars are independent.

A conjecture for the phase space density of several states of the relativistic H-atom has been made by one of us [9]. Here we restrict ourselves to the ground state in the non-relativistic limit. The conjecture reduces to

$$P_{\mathbf{pr}}(\mathbf{r},\mathbf{p}) = f(\mathcal{E}(\mathbf{r},\mathbf{p}), L(\mathbf{r},\mathbf{p})); \quad f(\mathcal{E},L) = \frac{2Le^{2/\mathcal{E}}}{\pi^3|\mathcal{E}|^3} = \frac{2}{\pi^3}\,LR^3e^{-2R}, \quad R = -\frac{1}{\mathcal{E}}. \tag{42}$$

The first task is to verify that the ground state density emerges after integrating over momenta. At given $\mathbf{r}$ one can take the p_z-axis along $\mathbf{r}$, so that

$$\mathbf{p} = p(\sin\mu\cos\nu, \sin\mu\sin\nu, \cos\mu), \quad p = \sqrt{\frac{2(R-r)}{rR}}, \tag{43}$$

with $r \le R \le \infty$, $0 \le \mu \le \pi$, $0 \le \nu \le 2\pi$. The volume element reads

$$\mathrm{d}^3p = \mathrm{d}p\mathrm{d}\mu\mathrm{d}\nu\, p^2\sin\mu = \mathrm{d}R\mathrm{d}\mu\mathrm{d}\nu\,\sqrt{\frac{2(R-r)}{rR^5}}\,\sin\mu. \tag{44}$$

Since $L = pr\sin\mu$, Eq. (42) indeed reproduces the QM result, viz.

$$P_{\mathbf{r}}(\mathbf{r}) = \int \mathrm{d}^3p\, P_{\mathbf{pr}}(\mathbf{r},\mathbf{p}) = \frac{4}{\pi}\int_r^\infty \mathrm{d}R(R-r)e^{-2R} = \frac{e^{-2r}}{\pi}. \tag{45}$$

This can indeed be written as

$$P_{\mathbf{r}}(\mathbf{r}) = \psi_0^2(r) Y_{00}^2(\theta,\phi), \quad \psi_0(r) = 2e^{-r}, \quad Y_{00}(\theta,\phi) = \frac{1}{\sqrt{4\pi}}, \tag{46}$$

and leads to $P_r(r) = r^2\psi_0^2(r) = 4r^2e^{-2r}$ with normalisation $\int_0^\infty \mathrm{d}r\, P_r(r) = 1$.

For $P_{\mathcal{E}L}(\mathcal{E}, L)$ we have the definition

$$\begin{aligned} P_{\mathcal{E}L}(\mathcal{E}, L) = & \int \mathrm{d}^3r \int \mathrm{d}^3p\, \delta(\underline{\mathcal{E}} - \mathcal{E})\delta(\underline{L} - L) P_{\mathbf{pr}}(\mathbf{p}, \mathbf{r}) \\ & = 4\pi f(\mathcal{E}, L) \int \mathrm{d}r\, r^2 \int_0^{2\pi} \mathrm{d}\nu \int_0^\pi d\mu \sqrt{\frac{2(R-r)}{rR}} \\ & \quad \times \sin\mu\, \delta\left(r\sqrt{\frac{2(R-r)}{rR}} \sin\mu - L \right) \end{aligned} \tag{47}$$

Hence, taking into account the contributions from $\mu = \bar{\mu} < \frac{1}{2}\pi$ and from $\mu = \pi - \bar{\mu}$,

$$P_{\mathcal{E}L}(\mathcal{E}, L) = 16\pi^2 f(\mathcal{E}, L) \int_{r_-}^{r_+} \mathrm{d}r\, \frac{rL\sqrt{R/2}}{\sqrt{rR - r^2 - \frac{1}{2}L^2R}}$$

Expressing $\kappa = kL$, that lies between 0 and 1, as

$$\kappa = \frac{L}{L_{\max}} = \frac{L}{\sqrt{R/2}} = kL = \sqrt{1-\varepsilon^2}, \tag{48}$$

and using that $r_\pm = \frac{1}{2}R(1 \pm \varepsilon)$, this reduces to

$$P_{\mathcal{E}L}(\mathcal{E}, L) = 8\sqrt{2}\frac{L^2}{|\mathcal{E}|^{9/2}} e^{-2/|\mathcal{E}|}\,, \tag{49}$$

where $L \le L_{\max}$. Because the latter depends on $\mathcal{E}$, the result does not factorize. However, since both ε and κ lie between 0 and 1, the weight $P_{\mathcal{E}L}(\mathcal{E}, L)\mathrm{d}\mathcal{E}\mathrm{d}L$ can be factored in the forms $P_{\mathcal{E}}(\mathcal{E})\mathrm{d}\mathcal{E}\, P_\varepsilon(\varepsilon)\mathrm{d}\varepsilon$ and $P_{\mathcal{E}}(\mathcal{E})\mathrm{d}\mathcal{E}\, P_\kappa(\kappa)\mathrm{d}\kappa$, where

$$\begin{aligned} P_{\mathcal{E}}(\mathcal{E}) &= \frac{4}{3|\mathcal{E}|^6} e^{-2/|\mathcal{E}|}\,, && (-\infty < \mathcal{E} < 0), \\ P_\varepsilon(\varepsilon) &= 3\varepsilon\sqrt{1-\varepsilon^2}, && (0 \le \varepsilon < 1), \\ P_\kappa(\kappa) &= 3\kappa^2, && (0 < \kappa \le 1). \end{aligned} \tag{50}$$

For numerical simulation of an ensemble of orbits, a properly distributed set of initial values can be gotten as follows. Choose randomly two independent random numbers u_1 and u_2 between 0 and 1 and equate R and κ from

$$(1 + 2R + 2R^2 + \frac{4}{3}R^3 + \frac{2}{3}R^4)e^{-2R} = u_1, \qquad \kappa = u_2^{1/3}, \tag{51}$$

and from them the other parameters that characterise the orbit.

A uniform distribution of u_1 and u_2 values produces the desired probability density, viz. $\mathrm{d}u_1\mathrm{d}u_2 = -\mathrm{d}\kappa\mathrm{d}R\, P_{\kappa R}(\kappa, R)$. For an ensemble of initial conditions, the task is to see whether this ensemble is dynamically stable. The initial orbit has perihelion and aphelion $r_\mp$ and can start at either of them.

The distribution of the physical momentum is

$$P_p(p) = \int \mathrm{d}^3 r\, P_{\mathbf{pr}}(\mathbf{p}, \mathbf{r}) \tag{52}$$

Taking and spherical coordinates with the z-axis parallel to $\mathbf{p}$, we have $L = pr\sin\theta$ and then from $\frac{1}{2}p^2 - 1/r = -1/R$

$$P_p(p) = \frac{2p}{\pi}\int_0^{2/p^2} \mathrm{d}r\, r^3 R^3 e^{-2R} = \frac{2p}{\pi}\int_0^\infty \mathrm{d}R\, \frac{R^6}{(1+\frac{1}{2}p^2R)^5} e^{-2R} \tag{53}$$

which is also properly normalised. Indeed, its integral over the $3d$ momentum can be written as

$$16\int_0^\infty \frac{\mathrm{d}x\, x}{(1+x)^5}\int_0^\infty \mathrm{d}R\, R^4 e^{-2R} = 1. \tag{54}$$

The limiting behaviours of $P_p(p)$ are $45p/4\pi$ for $p \to 0$ and $16/\pi p^9$ for $p \to \infty$.

The Wigner function is generally defined as

$$W(\mathbf{p}, \mathbf{r}) = \frac{1}{(2\pi)^3}\int \mathrm{d}^3 s\, \psi_0(\mathbf{r} - \frac{1}{2}\mathbf{s})\psi_0(\mathbf{r} + \frac{1}{2}\mathbf{s}) e^{i\mathbf{s}\cdot\mathbf{p}} \tag{55}$$

It implies $W_p(p) = \int \mathrm{d}^3\mathbf{r}\, W(\mathbf{p}, \mathbf{r})$, which yields $W_p(0) = 1$, to be compared with $P_p(0) = 0$. The distribution functions are physically different: the Wigner function deals with the statistical momentum and $P_{\mathbf{pr}}$ with the instantaneous momentum. Except for Gaussian distributions, W will have negative parts, while $P_{\mathbf{pr}}$ is always nonnegative.

4. Implementing the algorithm in OpenCL

We did make extensive use of GPGPU computing by writing our code in C++/OpenCL. This led to a factor 10^2 improvement in processing speed with respect to a normal auto-vectorized single core C++ implementation, which allowed us to simulate on the order of 10^7 modes in real time, allowing us to tackle the problem in 3D without making use of window approximations as was done in previous simulations (Cole&Zou 2003). In the next sections we will elaborate on how this led to vastly different results with respect to previous modeling work (Cole&Zou 2003).

We ran the simulations on a state of the art PC, consisting out of an Intel Core i7 2600k overclocked to 4.6 GHz (Core i7 4770k+ equivalent in performance), together

with 16 GB of RAM. In our earlier simulations we used an AMD HD6970 GPU, which was later upgraded to an AMD R9-290X GPU. This GPU delivers 5.6 TFLOPS of single precision floating point performance and 350 Gigabytes per second of memory bandwidth.

Solving the equation of motion is done with the Runge-Kutta fourth order ODE integration scheme. The most demanding part of this constitutes the summation of all modes of the E-field. This is where we use OpenCL. Since all these modes are independent of each other, we can sum them in parallel on the GPU. Basically we reduce this tremendous (10^7) sum into 10^4 sub sums, ordered in groups of size 256 sharing local memory on the GPU, divided over 1536/2816 stream processors. The final reduction step of the 10^4 sub sums is done on the CPU. This costs no extra time and has the advantage that the final reduction step can be done with double precision, while on the GPU it is done with single precision. We confirmed that our required numerical precision was met by comparing the parallel OpenCL GPU reduction with a normal double precision C++ CPU only reduction.

For the Runge-Kutta fourth order algorithm to remain stable on our timescales we found out that we need approximately $600 - 2000$ iterations per orbit for high eccentricities. In our code we used at least 4000 iterations per orbit, since solving the ODE, if the E-field is known, is computationally inexpensive. The catch is that we can not update this E-field so often, because every update involves a 10^7 sized reduction. For this reason we update the field only 10 times per period for the highest frequency mode in the spectrum. In between we use a 4^{th} order Lagrange Polynomial for interpolation to calculate the E-field.

Since the electron's energy can drop below the memory limit of our simulation ($\mathcal{E} = -1.6$), in such a case we artificially increase its energy by giving it a 'push' parallel to the electron's velocity vector. Naively, this shouldn't constitute a problem, since according to the conjecture of previous section the electron should stay out of this regime 99%+ of time. We tested that the electron can drop to very low energies like $\mathcal{E} = -4.0$, but the electron always seems to recover from this regime. However, we do observe that in this regime the angular momentum and eccentricity can change fast, possibly biasing our final results.

We ran our simulations for around $1-5\,10^6$ orbits for the different sets of harmonics (with or without a smooth window). This is many times more than the total run time of Cole&Zou 2003. See table 1 for the precise run times.

4.1. Results

4.1.1. Moving cutoff. Our first simulations utilised a 'moving' cutoff for the electric field. We took the cutoff at N_{harm} times the orbital frequency. We updated this cutoff frequency in increments of 20% as our orbit changed. This has the advantage that we do not introduce discontinuities in the Abraham-Lorentz equation of motion (10). For Z=3 experience shows that energy of the electron varies by a few percent every orbit

and thus the electric field is updated every 10^2 orbits.

Our most promising results were multiple simulations for $N_{\rm harm} = 2.5$ and $N = 1.5 * 10^6$ using either $Z = 1$ or $Z = 3$ (see figures 1-6). Initially it seemed that we obtained a stable solution, but instabilities, which eventually led to ionization of the atom, developed on timescales of the order $10^7 t_0$ for $N_{\rm harm} = 2.5$ and $Z = 3$. Higher harmonics (4.5 and 6.5) are unstable on even shorter timescales ($10^6 - 10^5 t_0$). We define ionisation as the moment when the electron stays above $\mathcal{E} = -0.05$ for a duration for at least $10^7 t_0$. The moment of ionisation is cut out of the subsequent plots.

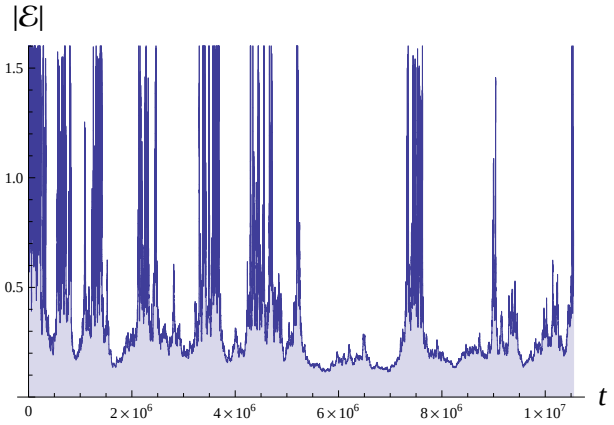

Figure 1. Energy of the electron as function of time for $Z = 3$, in Bohr units.

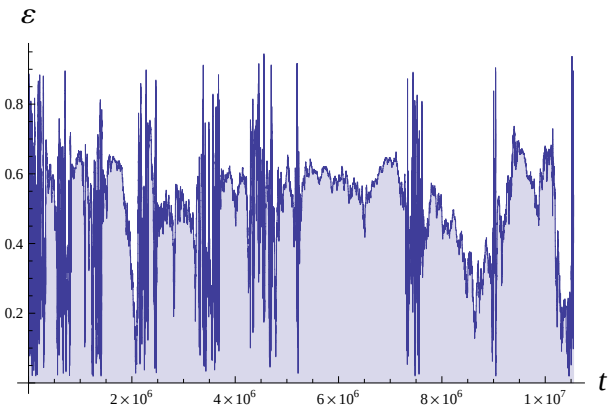

Figure 2. Eccentricity of the electron orbit as function of time for $Z = 3$, in Bohr units.

property	value	duration (s)
t_{total}	$1.2\,10^7\,t_0$	$3.2\,10^{-11}$ s
t_{damp}	$4.3\,10^5\,t_0$	$1.2\,10^{-12}$ s
N_{orbit}	$1.9\,10^6$	$1.0\ 10^6$
N_{damp}	28	

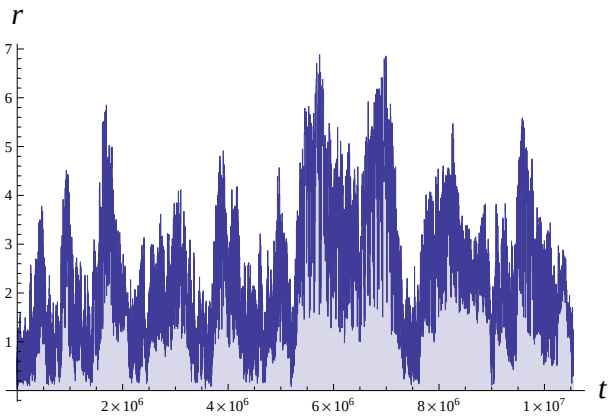

Figure 3. Radius of the electron orbit as function of time for $Z = 3$, in Bohr units.

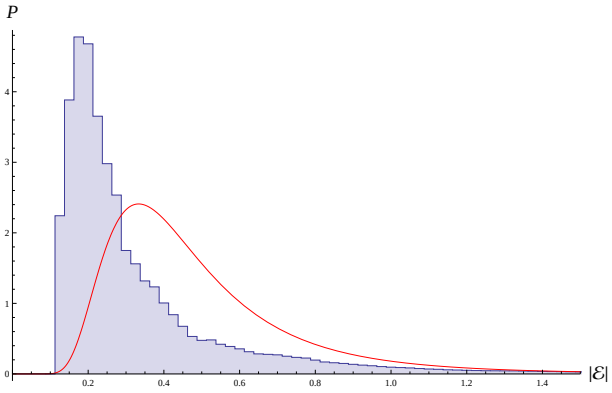

Figure 4. Normalised histogram of the electron energy for $Z = 3$ versus the conjecture, in Bohr units.

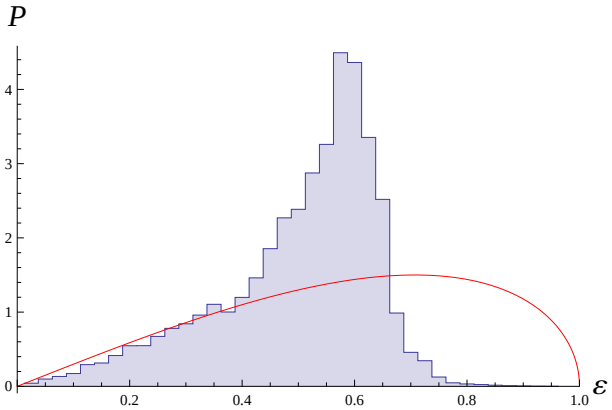

Figure 5. Normalised histogram of the eccentricity of the electron orbit for $Z = 3$ versus the conjecture, in Bohr units.

Table 1: Duration and number of orbits for our simulation with 2.5 harmonics and $Z = 3$. The classical period of a characteristic orbit is the Bohr period $t_0 = 2\pi\tau_0$. The number of orbits is first given as the total duration divided by t_0; its second entry is the actual number of orbits in the simulation. N_{damp} is the duration of the simulation expressed in damping times.

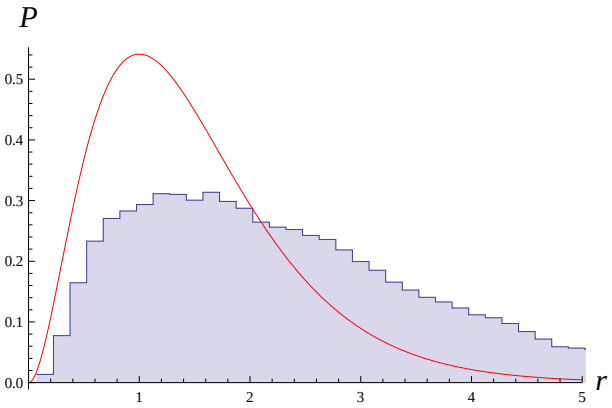

Figure 6. Normalised histogram of the radius of the electron orbit for $Z = 3$ versus the conjecture, in Bohr units

In these time series (figures 1,2,3) we see a rapid fluctuation of the energy and radius, while the eccentricity and angular momentum remain stable on longer timescales. Contrary to our expectations and the ones of Cole&Zou 2003, we fail to reproduce the 1s wavefunction on such long timescales. Comparing the angular momentum, eccentricity and energy distributions to our conjecture we fail to see high eccentricities, while we confirmed that our simulation can accurately handle eccentricities of at least ~ 0.99. The cause of the lack of these higher eccentricities remains unanswered so far.

One of the striking results from Cole&Zou 2003 was that they observed perfectly circular orbits. This was not true in our case and in strong contradiction with the previously discussed conjecture. Our explanation for this discrepancy is that Cole&Zou 2003 did run the simulation too short and thus missed variation of the angular momentum and eccentricity on longer timescales. Cole&Zou 2003 furthermore summed 11 simulations with the same initial conditions (circular orbit) but different seeds, which clearly is not a valid approach anymore and leads to wrong results (i.e., they chose a timescale much shorter than the timescale on which the eccentricity changes significantly). Furthermore a window approximation of 5% around the first harmonic of the E-field was used. We have verified that this leads to wrong results for even a single harmonic, since the E-field components outside the 'resonant' window of several percent seem to influence the angular momentum and eccentricity distributions on longer timescales. If we follow Cole&Zou by taking the data for $r(t)$ of Fig. 3 up to the smaller time $2.5\ 10^5/2\pi = 16,000$ orbits with a nearly circular orbit as initial condition, we get as radius distribution the data presented in Table 2:

property	value	total
t_{total}	$11 \times 6.21\,10^5 t_0$	$11 * 1.5\,10^{-11}$ s
t_{damp}	$3.8\,10^6 t_0$	$9.36\,10^{-11}$ s
N_{orbit}	$11 \times 1.0\,10^5$	
N_{damp}	11×0.16	

Table 2: Duration and number of orbits for the Cole&Zou simulation with $Z = 1$ and a 5% window around the first harmonic in 2D. The factor 11 is the number of different runs.

4.1.2. Fixed cutoff After we upgraded to a more powerful GPU, we ran simulations with a fixed cutoff on the frequency spectrum of the the random electric fields, so that we could keep the field and time step the same during the whole simulation. This cutoff was set at $N_{\rm harm} = 1.5$ harmonics for an energy of $\mathcal{E} = -1.6$ so that $N_{\rm harm} = 52$ harmonics occur at energy of $\mathcal{E} = -0.15$. Multiple configurations led to ionization in a rather short amount of time (10.000 orbits) . We observe that the energy of the electron goes to zero, while its eccentricity increases, before it ionizes (see figures 7-9) .

This is unphysical and raises questions about our numerical precision in the fixed cutoff case. Since we use double-precision, the machine precision is not our limiting factor. When the electron is close to the lower energy limit from the conjecture ($\mathcal{E} = -0.15$), though, we have to include 52 harmonics, in order that at the lower energy threshold of $\mathcal{E} = -1.6$ we retain the promised 1.5 harmonics. This means that integrated strength of the 52^{th} harmonic is ~ 2700 stronger than the integrated strength of the first harmonic. Hence we must keep our 4^{th} order interpolation error very small so that we correctly represent the integrated strength up to the first harmonic, which should be one of the most dominant ones, with the higher harmonics statistically averaging out. Our tests turned out that our 'numerical' error in this case can reach up to 20% of the integrated strength of the first harmonic. Since this is a small statistical error, we expect it to average out and not lead to too much systematic disruption of our data. We tested this further by experimenting with an exponential cutoff, which ranged in values from 1 at the lowest frequency in our spectrum to 0.1 at the cutoff frequency. No improvement of the electron stability was observed.

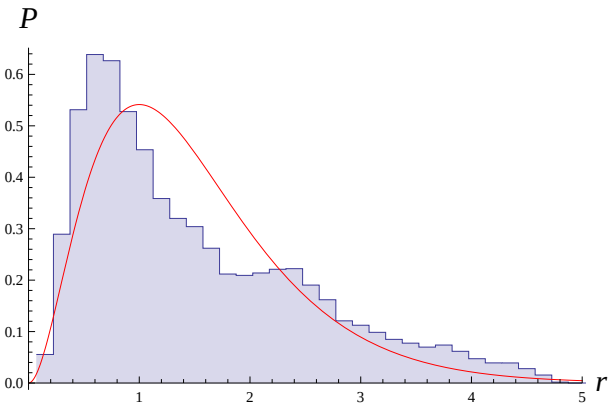

Figure 7. Normalised histogram of the radius of the electron orbit for $Z = 3$ versus the conjecture, in Bohr units. The data are taken from Fig. 3 for times up to $10^5 t_0$, corresponding to an estimated number 16,000 of orbits, about 100 times shorter than in Fig. 6.

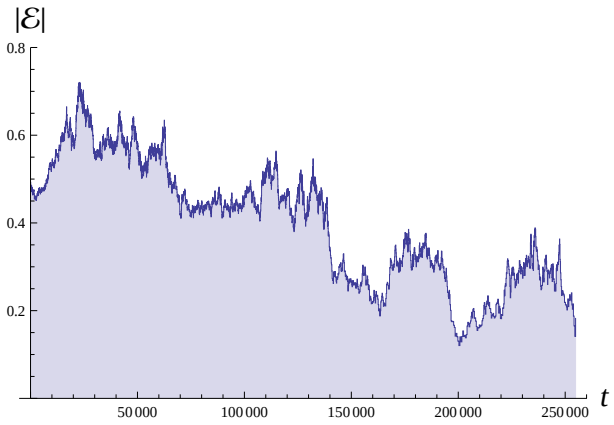

Figure 8. Energy as function of time for $Z = 1$ with a fixed cutoff exposing the trend towards ionisation at $\mathcal{E} = 0$, $\varepsilon = 1$. The time window is 45 times shorter than in Figures 1, 2 and 3.

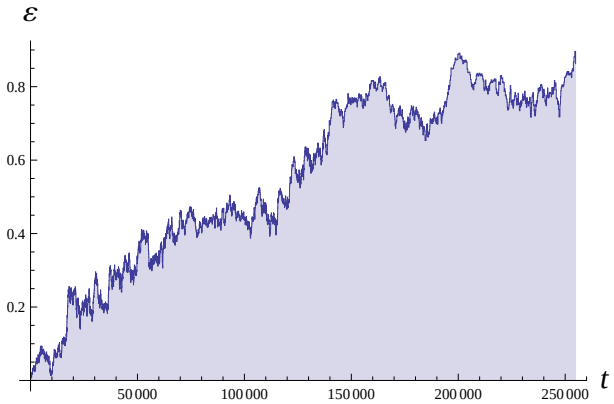

Figure 9. Eccentricity as function of time for $Z = 1$ with a fixed cutoff exposing the trend towards ionisation at $\mathcal{E} = 0$, $\varepsilon = 1$. The time window is 45 times shorter than in Figures 1, 2 and 3.

5. Summary and outlook

In this work we have considered the hydrogen ground state in Stochastic Electrodynamics (SED). The approach was made tractable by replacing the Gaussian random field, sums over $3D$ momenta, by $1D$ sums over frequencies with amplitudes chosen such that they reproduce the same correlation function in the limit where the frequency mesh vanishes ($N \to \infty$).

Using vastly improved computational resources compared to a decade ago and the possibility to parallelise the code into OpenCL, we could simulate up to much longer timescales than in Cole&Zou 2003. We considered simulations both with a fixed cutoff and with a moving cutoff frequency. The results show that even for a simple problem consisting out of a moving cutoff at 2.5 times the electron angular frequency, the promising results from Cole&Zou 2003 are not valid anymore on longer timescales. This result is robust against several variations that we implemented, such as the 'grand

canonical', 'mixed grand canonical' and other schemes of the dynamics presented in section 2, which allowed to test our numerical reproducibility. If we include more harmonics or if we use a fixed cutoff, the solution is unstable on even shorter timescales. Furthermore, the solutions fail to reproduce the 1s ground state correctly even prior to ionisation.

We suspect that the H atom suffers from the same problems as the free particle [15]. The energy $e^2\mathbf{A}^2/2mc^2$ is in quantum mechanics perceived as a renormalisation $\delta m_e c^2$ of the electron rest energy. In SED it is a dynamical energy, transferred by the $\mathbf{p}\cdot\mathbf{A}$ term in the Hamiltonian, that gives energy to the electron when time progresses. Its energy scale $\alpha m_e c^2$ is much larger than the Rydberg energy $\frac{1}{2}\alpha^2 m_e c^2$. It seems to us that this transfer of physical energy from the field to kinetic plus potential energy in the H atom causes the ionisation. One may wonder whether a compensation mechanism for this transfer exists.

An improvement to our approach is to include the magnetic field, the weak spatial dependence of the electric field and the effect of the spin-orbit coupling. They will be considered in the near future. Relativistic effects are important for the problem provided the electron comes close to the nucleus [16, 17]. Otherwise they appear in the structure of SED as small mechanical corrections to the Kepler problem, which makes us suspect that they do not significantly alter the present findings.

Appendix: Parallelising the code into OpenCL

OpenCL is an extension to C++ that makes it possible to parallelise the summation in equation (15). Normally the summation of the modes is performed within for loops, where all elements are summed serially on a single CPU. GPUs though are much faster ($\sim 30\times$) and share a much higher memory bandwidth ($\sim 20\times$) than CPUs. They are built up out of thousands of stream processors. Each of these stream processors is much weaker than a single CPU core (usually 2 to 4 cores per CPU), but taken together they are tens to hundreds of times faster than a CPU. To utilise this strength we used OpenCL to program our GPU. In the OpenCL paradigm our GPU is called a compute device. Since we possess a single GPU, we utilise only one compute device. This compute device posseses 44 compute units, which are subdivided over 4 16-wide SIMDs (Single instruction, multiple data). Thus there are $64 \times 4 \times 16 = 2816$ processing elements. Each of these compute units can process up to 40 wavefronts of GPU specific size 64 simultaneously, only limited by the register (GPR) and local memory size. Processing multiple wavefronts of data is done to hide memory latency.

The sum in equation (15) is then summed by all of these processing elements using parallel reduction. The global work size is defined by the total number of elements to sum. These elements are summed in workgroups of size 256, i.e., 4 times the wavefront size for an AMD GCN (Graphics core next) GPU. These workgroups share local memory, such that every work item reads in its value from the global memory and copies it to the local memory, where it is summed in 8 steps ($2^8 = 256$) within a workgroup. During

the first step the first 128 work items are summed with the last 128 work items in pairs of two. In this way the sum is reduced by a factor of 2 each step. This reduces the total sum by a factor of 256, after which the remainder is copied to pinned RAM memory via a PCI Express bus and summed by the CPU. Overall, the performance improvement amounts to a factor of 50-300 depending on the exact combination of CPU and GPU.

The OpenCL code is available upon request.

6. Acknowledgments

It is a pleasure to thank Erik van Heusden for much discussion.

[1] L de la Peña and A M Cetto, 1996 *The Quantum Dice: An Introduction to Stochastic Electrodynamics*, (Kluwer, Dordrecht)

[2] H E Puthoff 1987 *Ground state of hydrogen as a zero-point-fluctuation-determined state*, Phys. Rev. D 35, 3266

[3] Th M Nieuwenhuizen, 2010 *Is the contextuality loophole fatal for the derivation of Bell inequalities?* Found. Phys. 41, 580

[4] L de la Peña, A M Cetto and A Valdés Hernández, *The Emerging Quantum: The physics behind quantum mechanics*, (Springer, Berlin, 2015)

[5] L de la Peña, A M Cetto and A Valdés-Hernándes 2012 *Quantum behaviour derived as an essentially stochastic behaviour*, Physica Scripta T 151 014008

[6] A M Cetto and L de la Peña *Radiative corrections for the matter-zeropoint field system: establishing contact with quantum electrodynamics*, Physica Scripta T 151 014009

[7] H M França, A Kamimura, G A Barreto 2012 *The Schrödinger equation, the zero-point electromagnetic radiation and the photoelectric effect*, arXiv:1207.4076.

[8] T M Nieuwenhuizen, 2007 *The Pullback Mechanism in Stochastic Electrodynamics*, AIP Conf. Proc. 962, 148

[9] T M Nieuwenhuizen 2006 *Classical phase space density for the relativistic hydrogen atom*, AIP Conf. Proc. 810, 198

[10] T M Nieuwenhuizen 2014 *A subquantum arrow of time*, Journal of Physics: Conference Series 504 012008

[11] P Claverie and F Soto 1982 *Nonrecurrence of the stochastic process for the hydrogen atom problem in stochastic electrodynamics* J. Math. Phys. 23, 753

[12] L De la Peña-Auerbach and AM Cetto 1977, *Derivation of quantum mechanics from stochastic electrodynamics*, J. Math. Phys. 18, 1612

[13] T M Nieuwenhuizen 2013, unpublished.

[14] D C Cole and Y Zou, 2003 *Quantum mechanical ground state of hydrogen obtained from classical electrodynamics*, Physics Letters A 317, 14

[15] L de la Peña and A Jáuregui 1983 *Stochastic electrodynamics for the free particle*, J. Math. Phys. 24, 2751

[16] T. H. Boyer, 2003, *Comments on Cole and Zou's calculation of the hydrogen ground state in classical physics*, Foundations of Physics Letters, 16, 613

[17] T. H. Boyer, 2004, *Unfamiliar trajectories for a relativistic particle in a Kepler or Coulomb potential*, Am. J. Phys. 72, 992